Journal of Nuclear Materials 390–391 (2009) 123–126

Contents lists available at ScienceDirect

Journal of Nuclear Materials

journal homepage: www.elsevier.com/locate/jnucmat

'Mixed-material evolution analysis of the ITER divertor' ☆

J.N. Brooks *, J.P. Allain

Purdue University, 400 Central Drive, West Lafayette, IN 47907, USA

ARTICLE INFO

PACS:
52.40.Hf
28.52.Fa
52.55.Fa
52.65.y

ABSTRACT

Evolution of the ITER outer divertor target surface is analyzed for the case of wall-sputtered beryllium transported to an initially tungsten divertor. Coupled codes for the convective edge plasma, impurity transport, and mixed-surface sputtering, give the wall-source beryllium flux to the divertor, the sputtering erosion/redeposition response, and the resulting beryllium surface content/growth. The analysis shows zero net Be growth over most (~80%) of the divertor, due to high re-sputtering and reflection—with an equilibrium Be/W surface quickly formed (~10 s)—but with a region near the strike point having substantial (~1 nm/s) growth.

1. Introduction

Mixed-material plasma facing surfaces can obviously form in fusion devices that use more than one surface material, due to surface erosion and material transport. Surface changes can affect sputtering and plasma transient erosion, thermo-mechanical properties, and tritium codeposition. This issue is receiving attention via experiment, e.g. as summarized in [1], and modeling, e.g. for Be/C [2]. A Be/W mixing situation was studied in PISCES and shown to have complicated effects including multi alloy formation [1,3]. While modeling of alloy formation is extremely challenging, it is desirable to develop some estimate of divertor surface composition changes including time scales.

We study here the ITER Be-wall/W-divertor system. Refs. [4,5] analysis used the US OMEGA code package (UEDGE, DEGAS, WBC, TRIM-SP, etc.) to compute the sputter erosion of the ITER Be coated outer first wall and transport to various plasma facing surfaces including the ~50 cm long outer vertical divertor target. That analysis was for reference full power D–T shots with 100 MW power from the core to the edge plasma, and for convective plasma edge conditions. The next step, done here, is to examine the divertor response to the Be flux. In keeping with the uncertain nature of plasma convection models and the plasma solution in general, we use an average-particle transport method—with support from more detailed computations—coupled to a basic Be/W binary-collision cascade sputtering model. (A goal for future work is rigorous, full-distribution transport/surface-interaction model using full-dynamic/kinetic surface response modeling, e.g. to be implemented on supercomputers).

2. Method

2.1. W-MIX code

Sputtering of a pure-tungsten divertor was first assessed via detailed WBC code analysis. For the reference edge plasma solution [4,5]—with electron temperature and D–T ion flux at/to the outer divertor shown in Fig. 1—the net and gross erosion of tungsten is found to be negligible. Therefore, we can ignore the effect of tungsten sputtering on the surface evolution. However, the tungsten still has a major effect which is to influence the sputtering and reflection of beryllium from a mixed Be/W surface. A deterministic code, W-MIX, was developed to compute the time-dependent divertor surface response, using the following model:

The Be flux to a divertor segment '*i*' is the sum of the flux due to wall sputtering/transport and the redeposited flux due to sputtering and reflection from the divertor:

$$\Gamma^{\mathrm{in},i}_{\mathrm{Be}} = \Gamma^{i}_{\mathrm{Be\text{-}wall}} + \sum_{j=1}^{j\,\mathrm{max}} \Gamma^{\mathrm{out},j}_{\mathrm{Be,S}} A_{\mathrm{S}}(j,i) + \sum_{j=1}^{j\,\mathrm{max}} \Gamma^{\mathrm{out},j}_{\mathrm{Be,R}} A_{\mathrm{R}}(j,i) \quad (1)$$

where $\Gamma^{i}_{\mathrm{Be\text{-}wall}}$ is the flux from wall sputtering (including direct transport to the divertor and via wall-to-plasma-to-divertor transport). This source—as given by Ref. [5] analysis—is time independent. The second term on the rhs of (1)—varying with time due to changes in divertor surface composition—is the incident flux of Be to segment i resulting from sputtering of the divertor, where $\Gamma^{\mathrm{out},j}_{\mathrm{Be,S}}$ is the sputtered flux from segment '*j*' and $A_{\mathrm{S}}(j,i)$ is the redeposition matrix element giving the fraction of sputtered flux from segment *j* that is deposited on segment i. The last term in (1) is the analogous incident flux of Be resulting from reflection of Be, where $A_{\mathrm{R}}(j,i)$ is the redeposition matrix element for reflected material. (We distinguish here between Be self-sputtering and reflection, due to the

☆ Work supported by the US Department of Energy, Office of Fusion Energy.
* Corresponding author.
E-mail address: brooksjn@purdue.edu (J.N. Brooks).

0022-3115/$ - see front matter © 2009 Elsevier B.V. All rights reserved.
doi:10.1016/j.jnucmat.2009.01.138

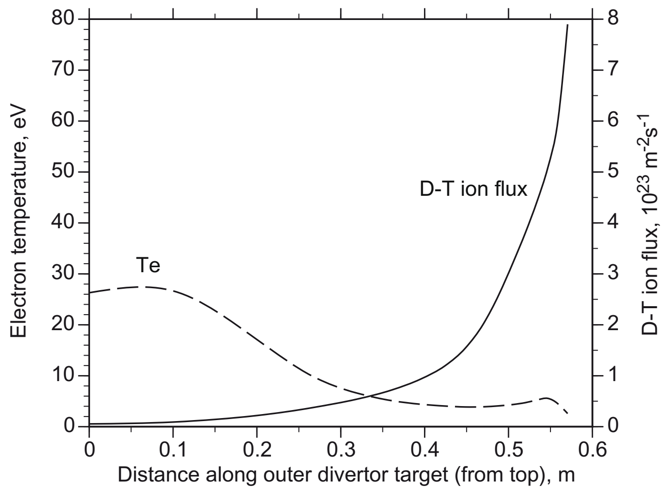

Fig. 1. Plasma parameters at the ITER outer vertical divertor target (strike point at ~0.55 m).

mixed-material surface and major differences in transport, sputtered atoms having higher local redeposition than reflected atoms, due to their lower emitted energy spectrum.)

The two redeposition matrices are supplied to W-MIX, via WBC code analysis, using the divertor geometry, 2-D edge plasma solution, and using time-independent sputtered and reflected atom energy and angular distributions from TRIM-SP calculations to be described. The use of time-independent matrices is acceptable for the present purposes since the emitted energy distributions (and resulting ionization distances of the emitted Be atoms) do not vary highly with surface composition/time, even though the sputter and reflection yields do vary significantly.

The sputtered Be flux from a divertor segment is:

$$\Gamma^{\mathrm{out},i}_{\mathrm{Be,S}} = \Gamma^i_{\mathrm{D}} Y^i_{\mathrm{D}} + \Gamma^i_{\mathrm{T}} Y^i_{\mathrm{T}} + \Gamma^i_{\mathrm{He}} Y^i_{\mathrm{He}} + \Gamma^{\mathrm{in},i}_{\mathrm{Be}} Y^i_{\mathrm{Be}}, \quad (2)$$

for incident particle flux Γ^i_{X}, sputter yield Y^i_{X}, and particle (ion) species X = D, T, He, Be. The D, T, and He fluxes are given by the convective edge plasma solution [3,4] assuming a D–T plasma with 5% helium.

The reflected flux from a divertor segment is:

$$\Gamma^{\mathrm{out},i}_{\mathrm{Be,R}} = \Gamma^{\mathrm{in},i}_{\mathrm{Be}} R^i_{\mathrm{Be}} \quad (3)$$

For reflection coefficient R^i_{Be} .

The sputter yields are a function of particle incidence energy and angle, and the local time-dependent surface composition, the latter characterized by the Be atom fraction 'f' in an incident particle interaction depth, i.e.

$$Y^i_{\mathrm{X}} = Y^i_{\mathrm{X}}(E^i_{\mathrm{X}}, \theta^i_{\mathrm{X}}, f^i). \quad (4)$$

Likewise for the Be reflection coefficient:

$$R^i_{\mathrm{Be}} = R^i_{\mathrm{Be}}(E^i_{\mathrm{Be}}, \theta^i_{\mathrm{Be}}, f^i). \quad (5)$$

A supporting sheath analysis shows spatially-invariant average incidence angles for the particle species considered of about 52° from the normal (with small variance), and this is used in the sputtering and reflection calculations. Also used is the particle average energy determined by the locally-varying pre-sheath energy and sheath-acquired energy. For self-sputtering the yield is determined by convolution over the incident Be from the three sources treated (wall sputtering, divertor sputtering, and divertor reflection) due to their different charge states and sheath-acquired-energies.

The net Be flux to the divertor is given by deposition minus erosion and reflection, to determine the Be accumulation at each segment:

$$\Gamma^{\mathrm{net},i}_{\mathrm{Be}} = \Gamma^{\mathrm{in},i}_{\mathrm{Be}} - \Gamma^{\mathrm{out},i}_{\mathrm{Be,S}} - \Gamma^{\mathrm{out},i}_{\mathrm{Be,R}}. \quad (6)$$

The Be fraction is found from a simple mixing model, assuming a fixed interaction zone of depth d_0 for implantation and sputtering (of roughly the D^+, etc. penetration distance), and using fixed respective atom densities for Be and W. For this model the equivalent thickness of deposited beryllium in the interaction zone, at time t, is given by:

$$d^i_1(t) = d^i_1(t - \Delta t) + \Gamma^{\mathrm{net},i}_{\mathrm{Be}} \Delta t \rho_{\mathbf{Be}}, \quad (7)$$

subject to $0 \leqslant d^i_1(t) \leqslant d_0$ and initial condition $d^i_1(0) = 0$, and for Be atom density ρ_{Be}

The equivalent tungsten thickness is $d^i_2 = d_0 - d^i_1$

The Be surface fraction in depth d_0 is then:

$$f^i = \frac{d^i_1 \rho_{\mathrm{Be}}}{d^i_1 \rho_{\mathrm{Be}} + d^i_2 \rho_{\mathrm{W}}}. \quad (8)$$

For (8) we use d_0 = 10 nm and Be and W theoretical densities. (Variations in d_0 affect the time constants but with little effect on the equilibrium net erosion solution).

The W-MIX code solves (1)–(8), for the 17 point UEDGE divertor grid, for a single time, by iteration, and then advances the system in time, updating the f^i array and sputter and reflection coefficients at each time step. The code is run until equilibrium surface composition is reached.

2.2. Be/W sputter and reflection yields

For the plasma regime considered the irradiation of a mixed Be-W surface by light-particles results in the highly dominant sputtering of Be. This is primarily due to the Be/W disparate-mass, with resulting large binary-collision differences in energy transfer to Be atoms compared to W. This simple kinematic result provides reasonable justification for our present use of the static code TRIM-SP [6] to compute sputter yields for the mixed-surface. The simulations do not include kinetic-dependent or chemical-dependent effects such as phase transformations or chemical composition evolution via diffusion (e.g. as discussed in [1] to predict the formation and stability of certain phases under irradiation such as BeW_2, $Be_{12}W$ or $Be_{22}W$).

TRIM-SP simulations were run for D, T, He and Be bombardment for energies between 10 and 1000 eV (higher than needed for the present W-MIX runs but included for completeness), and at 52° incidence. Runs were made for a 100 nm uniform mixed-surface, with most interactions occurring within the first 10 nm. The mass density was linearly weighted based on the fractional composition of Be to total (Be + W) atoms. Similarly, the surface binding energy was weighted and the bond energy was taken as 10% of the heat of sublimation. (Comparative simulations used a binding energy of 1 eV and found the results varied by at most 5–10%). Each run used 10000 flights.

Fig. 2 shows the dependence of the mixed-material sputter yield on the Be atom fraction for D incidence. Except of course for the pure-tungsten (f = 0) case, the sputtering is entirely or mostly Be. The Be sputter yield varies about linearly with f, for incident energy >100 eV, and is non-linear for lower energies. Yields for the other particles (T, He, Be) have similar trends.

Results for reflection show, as expected, much higher reflection of Be from tungsten-containing surfaces compared to a pure-Be surface. For example, for ~200 eV Be (impinging on about the top 20 cm of the target), the reflection coefficient of ~0.6 for f = 0.2 is about three times higher than for a pure Be target.

3. Surface evolution

3.1. Reference Case

Fig. 3 shows the W-MIX computed divertor surface evolution. Starting from a pure tungsten surface at time zero, equilibrium is reached in about 30 s. Fig. 4 shows the net Be growth rate at equilibrium and the gross growth rate due solely to wall-to-divertor transfer (i.e. with no divertor sputtering/reflection, and including transfer via wall-to-plasma-to divertor). (The gross rate curve in Fig. 4 arises from a wall-source Be to plasma-source D–T ion flux ratio varying from ~6% at the target top, to ~0.02% at the strike point). In spite of significant beryllium flux from the wall most of the surface remains as tungsten, with a stable mixed Be/W overlayer forming quickly.

The reason for the zero net growth region is that Be is removed as fast as it impinges, by sputtering and reflection. In contrast, Be does build up on part of the lower portion of the divertor. This growth is due to: (1) transfer of Be from top-to-bottom, from a step-to-step erosion/redeposition process, and (2) lower sputter yields and higher sputter and reflection redeposition fractions for the lower temperature, higher density strike point region (this offsetting the higher D–T flux). (The local Be growth minimum near the strike point occurs because of a fine balance between sputtering and deposition; this is highly dependent on near-threshold sputter yields and hence on model-dependent plasma temperature/particle energy values in this region). The peak growth rate of order 1 nm/s is substantial, implying a roughly 1 μm thick Be coating after a 400–1000 s ITER shot.

Another result of interest concerns the fate of non-divertor redeposited Be. This is computed to be about 50% of the impinging Be. While not tracked in detail in this study it appears that this material would tend to deposit below the divertor. Implications for T/Be codeposition in this colder region of ITER are under analysis.

3.2. Variations

Fig. 5 shows the divertor response to different Be wall sources, $\Gamma^{i}_{\text{Be-wall}}$, corresponding to variations in impurity convection models as defined in Ref [5]. The results are qualitatively similar to the reference case, showing no growth on the top half of the divertor target and growth near the strike point. The growth area and peak

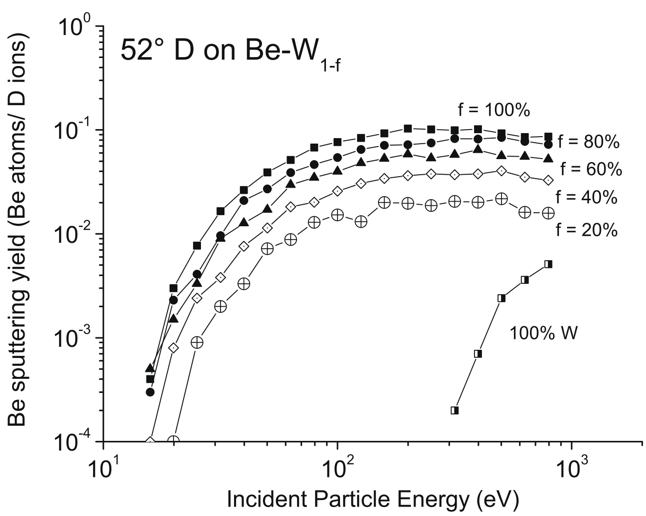

Fig. 2. Beryllium sputter yield from mixed Be/W surface as a function of fractional Be composition (W sputter yield shown for $f = 0$ case). TRIM-SP computation, 100 nm mixed-surface, 52° (from normal) D incidence.

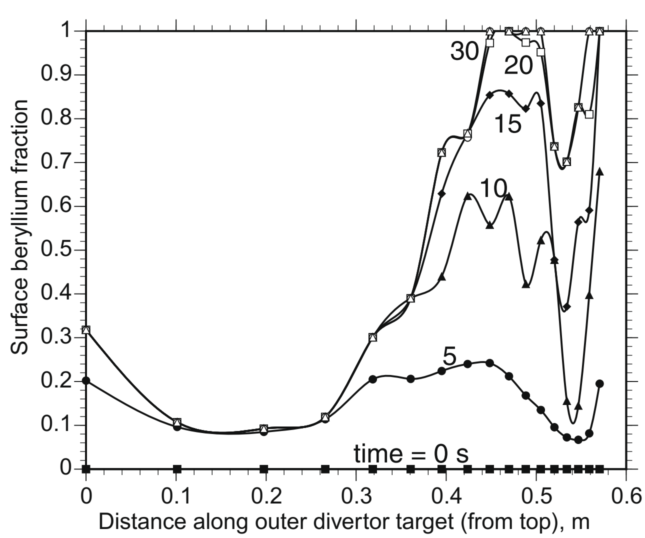

Fig. 3. Time dependence of the Be fraction in the top 10 nm of the divertor surface.

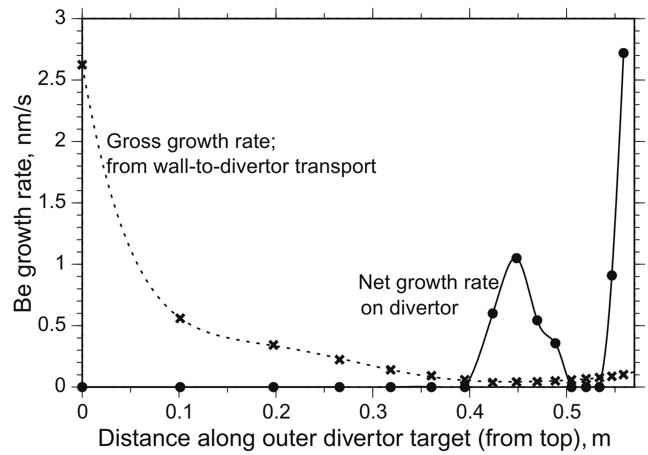

Fig. 4. Net Be growth rate at equilibrium (⩾30 s) and gross rate from wall-to-divertor transport.

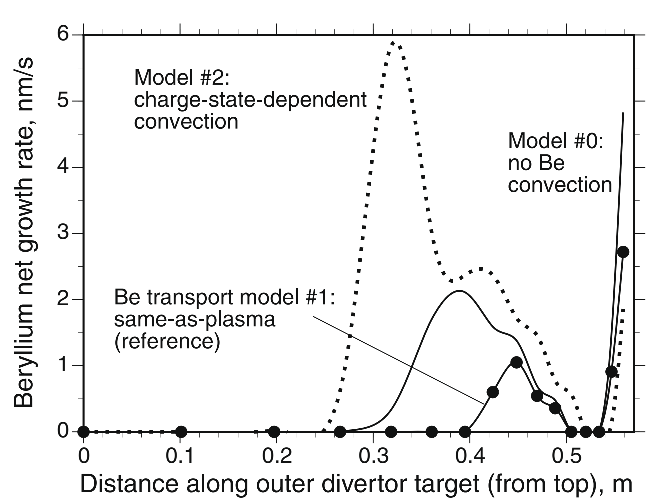

Fig. 5. Net growth rate for various wall-sputtered impurity transport models.

rates increase due to higher wall-sputtered Be transport to the divertor for the variations shown.

To assess the sensitivity to Be reflection coefficients we ran a case with zero reflection. The resulting growth region is about twice as big (from ~30-55 cm) as for the reference case but with similar peak growth rate. Also, there is a significant reduction (~×2) in the Be lost from the wall/divertor system. Therefore, we conclude that reflection is important to the mixing process.

Analysis of surface temperature effects is planned for future study, however, we note here that high temperatures at/near the strike point would tend to limit the formation of a thick pure-Be growth layer, e.g. by evaporation, with a preliminary estimate showing likely transport of such evaporated Be to the device bottom.

4. Conclusions

This work examines Be/W mixing at the ITER outer vertical divertor target using a combination of impurity sputtering, reflection, and transport models, and a first-order mixing model, but without alloying and thermal/kinetic effects. Results show:

1. In spite of high Be flux to the divertor from wall sputtering a thick Be layer will not form over most of the divertor due to sputtering by the plasma and self-sputtering/reflection.
2. A thick Be layer can quickly form at/near the strike point, with ~1 μm Be depositing after only a single ITER plasma shot.
3. Significant Be would likely deposit on colder non-divertor surfaces due to sputter/transport from the divertor.

Required near-term modeling work in this area includes analysis of thermal/kinetic effects, ELM effects, and ongoing edge/SOL plasma analysis coupled to impurity transport. Longer term work should couple multi time-scale atomistic simulations with kinetic modeling, and eventually alloy modeling. Additional supporting experiments and code validation efforts are clearly needed.

Acknowledgements

We thank Purdue University undergraduate students B. Hollybee and S. Ortoleva for help with the TRIM-SP runs.

References

[1] R.P. Doerner, J. Nucl Mater. 363–365 (2007) 32.
[2] A. Kirshner et al., J. Nucl. Mater. 363–365 (2007) 91.
[3] M.J. Baldwin et al., J. Nucl. Mater. 363–365 (2007) 1179.
[4] T.D. Rognlien et al., J. Nucl. Mater. 363–365 (2007) 658.
[5] J.N. Brooks, J.P. Allain, T.D. Rognlien, Phys. Plasmas 13 (2006) 122502.
[6] W. Eckstein, Computer Simulation of Ion–Solid Interactions, Springer, Berlin, 1981.